

Cavity quantum electro-optics. II. Input-output relations between traveling optical and microwave fields

Mankei Tsang*

*Department of Electrical and Computer Engineering,
National University of Singapore, 4 Engineering Drive 3, Singapore 117576
Department of Physics, National University of Singapore, 2 Science Drive 3, Singapore 117542 and
Center for Quantum Information and Control, University of New Mexico,
MSC07-4220, Albuquerque, New Mexico 87131-0001, USA*

(Dated: October 29, 2018)

In the previous paper [M. Tsang, Phys. Rev. A **81**, 063837 (2010)], I proposed a quantum model of a cavity electro-optic modulator, which can coherently couple an optical cavity mode to a microwave resonator mode and enable novel quantum operations on the two modes, including laser cooling of the microwave mode, electro-optic entanglement, and backaction-evading optical measurement of a microwave quadrature. In this sequel, I focus on the quantum input-output relations between traveling optical and microwave fields coupled to a cavity electro-optic modulator. With red-sideband optical pumping, the relations are shown to resemble those of a beam splitter for the traveling fields, so that in the ideal case of zero parasitic loss and critical coupling, microwave photons can be coherently up-converted to “flying” optical photons with unit efficiency, and vice versa. With blue-sideband pumping, the modulator acts as a nondegenerate parametric amplifier, which can generate two-mode squeezing and hybrid entangled photon pairs at optical and microwave frequencies. These fundamental operations provide a potential bridge between circuit quantum electrodynamics and quantum optics.

PACS numbers: 42.50.Pq, 42.65.Ky, 42.65.Lm, 42.79.Hp

I. INTRODUCTION

The rapid recent progress in circuit quantum electrodynamics (QED) [1] has motivated the question of how superconducting microwave circuits can be interfaced with quantum optics technology for long-distance quantum information transfer. This task requires efficient and coherent frequency conversion between microwave and optical photons. Existing proposals involve the use of mechanical oscillators as mediators between electrical and optical systems [2], but a more straightforward way is to take advantage of the well known Pockels electro-optic effect in a noncentrosymmetric material, such as lithium niobate [3]. The Pockels effect is the change in the optical index of refraction of a material under an applied voltage. A Pockels cell can be satisfactorily modeled as a broadband second-order nonlinear optical medium and a capacitor on the electrical side [3], so the effect is inherently coherent and suitable for quantum optics experiments, much like the use of second-order nonlinear crystals in optical parametric amplifiers and oscillators. In the classical regime, high-quality cavity electro-optic modulators that can resonantly couple microwave and optical fields have been extensively studied and experimentally demonstrated [4–7], but a quantum analysis of the photon frequency conversion problem is still lacking.

In the previous paper [8], I have developed a quantum model of cavity electro-optic modulators that can be used to address the frequency conversion problem. While the previous paper focuses on the analogy between electro-optics and optomechanics and the interactions between resonator modes, the present paper studies the relations between the traveling microwave and optical fields coupled to the cavities and the conversion efficiencies in the presence of parasitic losses. I consider two modes of operations: red-sideband optical pumping and blue-sideband optical pumping. Red-sideband pumping in the classical regime has been considered previously in Refs. [7] with the assumption that the microwave field is undepleted; here I shall do a quantum analysis assuming that the optical pump is undepleted instead and allow the microwave fields and the up-converted optical fields to exchange energy. This process is shown to be a fundamentally noiseless operation resembling that of a variable beam-splitter, so that in the ideal case of zero parasitic loss and critical coupling, microwave photons can be coherently converted to optical photons with unit efficiency, and vice versa. With blue-sideband pumping, the electro-optic modulator acts as a nondegenerate parametric amplifier, which can generate two-mode squeezing and hybrid entangled photon pairs at optical and microwave frequencies.

*Electronic address: mankei@unm.edu

Given the fundamental importance of beam-splitters and parametric amplifiers in quantum optics [9], such operations enabled by the cavity electro-optic modulator should be similarly useful for future quantum optical interconnect technology, if the technical challenges of implementing a quantum-efficient cavity electro-optic modulator can be overcome.

II. MODEL

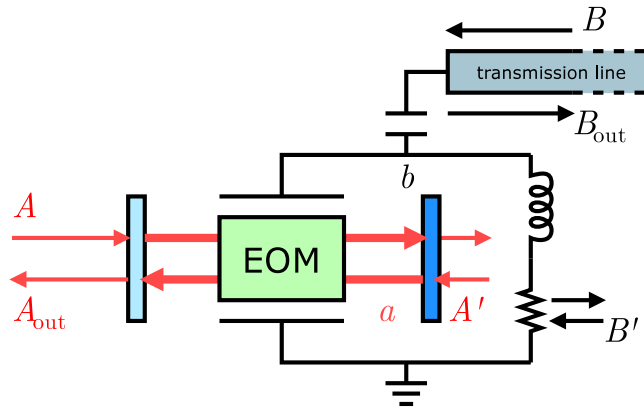


FIG. 1: (Color online). Schematic of a cavity electro-optic modulator coupled to traveling fields. The physics remains essentially the same regardless of the actual types of the optical and microwave resonators.

As shown in Fig. 1, the cavity electro-optic modulator model considered here is a generalization of the one in Ref. [8] and also includes traveling optical and microwave fields coupled to the optical and microwave resonators. A and A_{out} are the input and output optical field annihilation operators, B and B_{out} are the input and output microwave field annihilation operators, A' and B' are the quantum Langevin operators coupled through parasitic losses in the optical and microwave resonators [9], and a and b are the optical and microwave resonator-mode annihilation operators with resonance frequencies $\omega_{a,b}$. The relevant commutation relations are

$$[A(t), A^\dagger(t')] = \delta(t - t'), \quad (2.1)$$

$$[B(t), B^\dagger(t')] = \delta(t - t'), \quad (2.2)$$

$$[A'(t), A'^\dagger(t')] = \delta(t - t'), \quad (2.3)$$

$$[B'(t), B'^\dagger(t')] = \delta(t - t'), \quad (2.4)$$

$$[a, a^\dagger] = 1, \quad (2.5)$$

$$[b, b^\dagger] = 1. \quad (2.6)$$

In the following, I shall consider optical pumping at frequency $\omega_a - \omega_b$ or $\omega_a + \omega_b$. Following the terminology of optical parametric oscillators, I shall call the configuration *doubly resonant* (referring to the resonances at ω_a and ω_b) if the optical cavity is off-resonant at the pump frequency and *triply resonant* if the cavity is also resonant at the pump frequency.

III. RED-SIDEBAND OPTICAL PUMPING

A. Laplace analysis

Consider first red-sideband optical pumping at a frequency $\omega_a - \omega_b$, as depicted in Fig. 2. Assume that the optical cavity is off-resonant at $\omega_a - 2\omega_b$, so that the interactions between the pump and the optical field at $\omega_a - 2\omega_b$ can be neglected. This can be achieved for a Fabry-Pérot or whispering-gallery-mode cavity if ω_b does not coincide with the free spectral range, so that the pump is off-resonant in a doubly resonant configuration [8], or if the pump and the optical mode at ω_a are modes with different polarizations in a triply resonant configuration [7]. The resulting

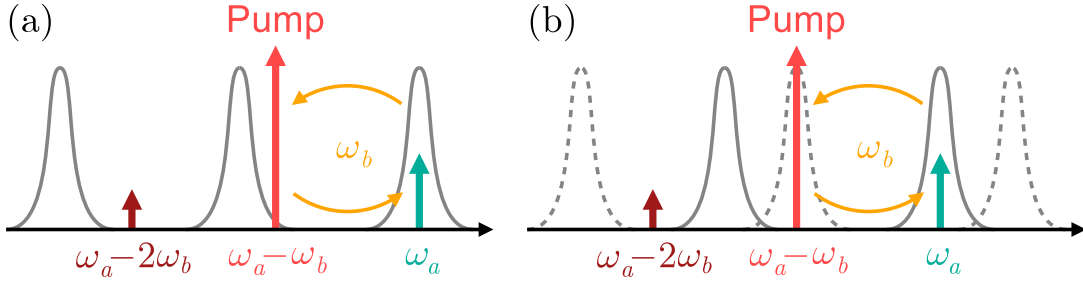


FIG. 2: (Color online). Red-sideband optical pumping schemes. (a) a doubly-resonant configuration with an off-resonant pump. (b) a triply-resonant configuration with a resonant pump in a different polarization mode [7]. Both schemes suppress interactions with the off-resonant field at $\omega_a - 2\omega_b$.

equations of motion in an appropriate rotating frame become

$$\frac{da}{dt} = ig\alpha b - \frac{\Gamma_a}{2}a + \sqrt{\gamma_a}A + \sqrt{\gamma'_a}A', \quad (3.1)$$

$$\frac{db}{dt} = ig\alpha^*a - \frac{\Gamma_b}{2}b + \sqrt{\gamma_b}B + \sqrt{\gamma'_b}B', \quad (3.2)$$

$$A_{\text{out}} = \sqrt{\gamma_a}a - A, \quad (3.3)$$

$$B_{\text{out}} = \sqrt{\gamma_b}b - B. \quad (3.4)$$

where

$$g \equiv \frac{\omega_a n^3 r l}{c \tau d} \left(\frac{\hbar \omega_b}{2C} \right)^{1/2} \quad (3.5)$$

is the electro-optic coupling coefficient in units of Hertz [8], n is the optical index of refraction inside the electro-optic medium, r is the electro-optic coefficient in units of m/V [3], l is the length of the medium, d is the thickness, τ is the optical round-trip time, C is the capacitance of the microwave resonator, $\Gamma_{a,b}$ are the total decay rates of the optical and microwave modes and are sums of the traveling-field coupling rates $\gamma_{a,b}$ and parasitic decay rates $\gamma'_{a,b}$, viz.,

$$\Gamma_a = \gamma_a + \gamma'_a, \quad \Gamma_b = \gamma_b + \gamma'_b, \quad (3.6)$$

and α is the normalized pump field amplitude, such that $|\alpha|^2$ is the number of pump photons inside the cavity.

Equations (3.1)-(3.4) are most easily solved using the Laplace transform, viz.,

$$\tilde{f}(s) \equiv \int_0^\infty dt f(t) \exp(-st), \quad (3.7)$$

so that, for example,

$$\frac{da(t)}{dt} \rightarrow s\tilde{a}(s) - a(0). \quad (3.8)$$

The solutions for A_{out} and B_{out} in the Laplace domain are given by

$$\begin{pmatrix} \tilde{A}_{\text{out}}(s) \\ \tilde{B}_{\text{out}}(s) \end{pmatrix} = \begin{pmatrix} F_{Aa}(s) & F_{Ab}(s) \\ F_{Ba}(s) & F_{Bb}(s) \end{pmatrix} \begin{pmatrix} a(0) \\ b(0) \end{pmatrix} + \begin{pmatrix} S_{AA}(s) & S_{AB}(s) & S_{AA'}(s) & S_{AB'}(s) \\ S_{BA}(s) & S_{BB}(s) & S_{BA'}(s) & S_{BB'}(s) \end{pmatrix} \begin{pmatrix} \tilde{A}(s) \\ \tilde{B}(s) \\ \tilde{A}'(s) \\ \tilde{B}'(s) \end{pmatrix}. \quad (3.9)$$

The first part of the solution that depends on an F matrix, $a(0)$, and $b(0)$ is the transient solution. Explicitly, the F matrix is given by

$$F(s) = \frac{1}{D(s)} \begin{pmatrix} \sqrt{\gamma_a} \left(s + \frac{\Gamma_a}{2} \right) & i\sqrt{\gamma_a}g\alpha \\ i\sqrt{\gamma_b}g\alpha^* & \sqrt{\gamma_b} \left(s + \frac{\Gamma_b}{2} \right) \end{pmatrix}, \quad (3.10)$$

where the denominator is

$$D(s) \equiv \left(s + \frac{\Gamma_a}{2}\right) \left(s + \frac{\Gamma_b}{2}\right) + |g\alpha|^2 \quad (3.11)$$

$$= (s - p_+)(s - p_-). \quad (3.12)$$

The poles of the transfer functions p_{\pm} , given by

$$p_{\pm} \equiv -\frac{\Gamma_a + \Gamma_b}{4} \pm \sqrt{\left(\frac{\Gamma_a - \Gamma_b}{4}\right)^2 - |g\alpha|^2}, \quad (3.13)$$

play a crucial role in the system dynamical response. Figure 3, the so-called root-locus plot [10], shows the loci of the poles on the complex plane as $|g\alpha|$ is increased. This plot is typical of a damped harmonic oscillator. When

$$|g\alpha| > \frac{|\Gamma_a - \Gamma_b|}{4}, \quad (3.14)$$

the poles become complex, indicating a phenomenon analogous to Rabi splitting [9]. The coupled electro-optic response then becomes oscillatory.

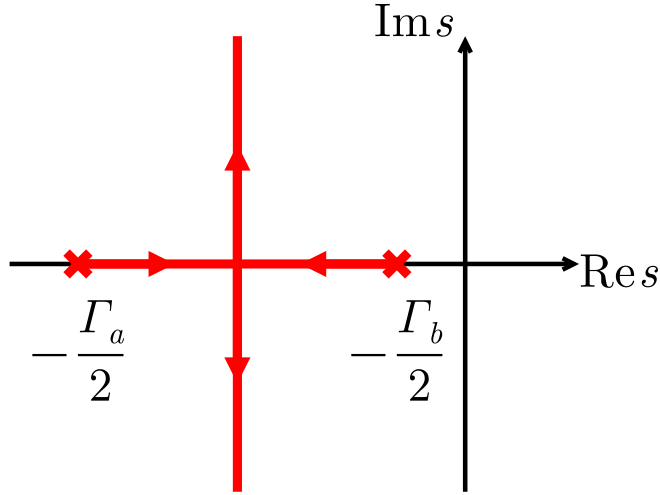


FIG. 3: (Color online). Root-locus plot for increasing red-sideband pump strength $|g\alpha|$.

B. Electro-optic beam-splitting

While the transient solution can be relevant to the task of reading out resonator modes, the S matrix, which relates the traveling fields, is of more interest to frequency conversion:

$$S(s) = \frac{1}{D(s)} \begin{pmatrix} \left(-s + \frac{\gamma_a - \gamma'_a}{2}\right) \left(s + \frac{\Gamma_b}{2}\right) - |g\alpha|^2 & ig\alpha\sqrt{\gamma_a\gamma_b} & \sqrt{\gamma_a\gamma'_a} \left(s + \frac{\Gamma_b}{2}\right) & ig\alpha\sqrt{\gamma_a\gamma'_b} \\ ig\alpha^*\sqrt{\gamma_a\gamma_b} & \left(-s + \frac{\gamma_b - \gamma'_b}{2}\right) \left(s + \frac{\Gamma_a}{2}\right) - |g\alpha|^2 & ig\alpha^*\sqrt{\gamma'_a\gamma_b} & \sqrt{\gamma_b\gamma'_b} \left(s + \frac{\Gamma_a}{2}\right) \end{pmatrix}. \quad (3.15)$$

The spectral behavior of the system is obtained by neglecting the transient solution and substituting $s = -i\omega$ in the S matrix, where ω is the detuning with respect to the carrier frequencies $\omega_{a,b}$. The Fourier transforms of the input

and output fields are related by the $S(-i\omega)$ matrix:

$$\hat{f}(\omega) \equiv \int_{-\infty}^{\infty} dt f(t) \exp(i\omega t), \quad (3.16)$$

$$\begin{pmatrix} \hat{A}_{\text{out}}(\omega) \\ \hat{B}_{\text{out}}(\omega) \end{pmatrix} = \begin{pmatrix} S_{AA}(-i\omega) & S_{AB}(-i\omega) & S_{AA'}(-i\omega) & S_{AB'}(-i\omega) \\ S_{BA}(-i\omega) & S_{BB}(-i\omega) & S_{BA'}(-i\omega) & S_{BB'}(-i\omega) \end{pmatrix} \begin{pmatrix} \hat{A}(\omega) \\ \hat{B}(\omega) \\ \hat{A}'(\omega) \\ \hat{B}'(\omega) \end{pmatrix}. \quad (3.17)$$

Equation (3.17) then resembles the spectral-domain input-output relations for a lossy beam splitter with quantum Langevin noise fields \hat{A}' and \hat{B}' [11].

For frequency conversion, the most important quantity is the electro-optic conversion efficiency, defined by

$$R(\omega) \equiv |S_{AB}(-i\omega)|^2 = |S_{BA}(-i\omega)|^2 \quad (3.18)$$

$$= \frac{|g\alpha|^2 \gamma_a \gamma_b}{|(-i\omega - p_+)(-i\omega - p_-)|^2}. \quad (3.19)$$

At zero detuning ($\omega = 0$),

$$R(0) = \frac{4\eta G_0}{(1 + G_0)^2}, \quad (3.20)$$

where

$$G_0 \equiv \frac{4|g\alpha|^2}{\Gamma_a \Gamma_b} \quad (3.21)$$

is analogous to the *cooperativity parameter* in cavity QED [12] and

$$\eta \equiv \frac{\gamma_a \gamma_b}{\Gamma_a \Gamma_b} \quad (3.22)$$

is the intrinsic efficiency of the system.

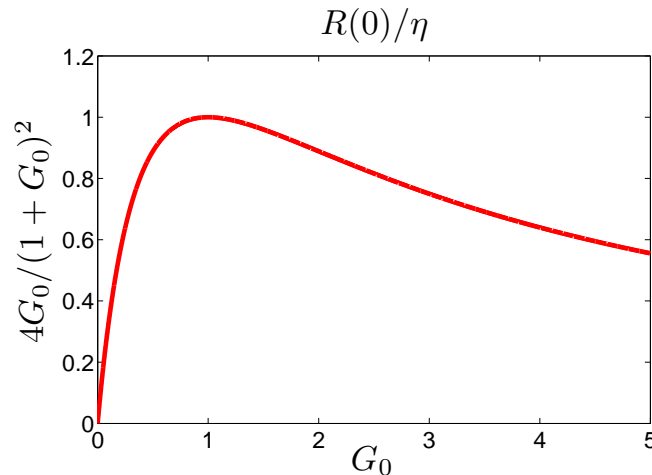


FIG. 4: (Color online). Conversion efficiency $R(0)/\eta$ at zero detuning versus the cooperativity parameter G_0 .

Figure 4 plots the conversion efficiency $R(0)/\eta$ at zero detuning. The highest efficiency at zero detuning is achieved when

$$G_0 = 1, \quad R(0) = \eta. \quad (3.23)$$

Since the zero-detuning efficiency drops when $G_0 > 1$, $G_0 = 1$ can be regarded as a *critical coupling* condition. For other frequencies, the efficiency given by Eq. (3.19) depends on the product of the distances between $-i\omega$ and the

poles p_{\pm} on the complex plane. Figure 5 plots the conversion efficiency with respect to the normalized detuning frequency $\Omega \equiv 2\omega/\sqrt{\Gamma_a\Gamma_b}$ and increasing G_0 , showing that the highest efficiencies indeed occur at frequencies near the poles. The conversion bandwidth is thus maximum when the imaginary parts of the poles are the farthest apart. For a fixed $|g\alpha|^2$, this means that

$$\Gamma_a = \Gamma_b, \quad (3.24)$$

and the resonators should ideally have the same decay rates. Figure 6, which plots the efficiency at critical coupling against $\ln(\Gamma_b/\Gamma_a)$, confirms this behavior.

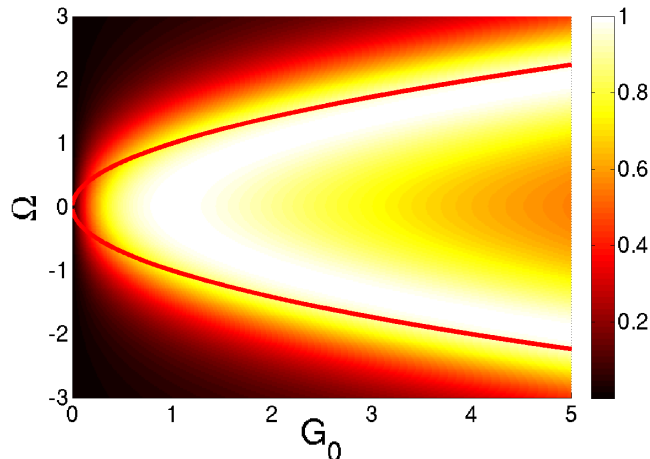


FIG. 5: (Color online). The color plot shows the conversion efficiency $R(\omega)/\eta$ at $\Gamma_a = \Gamma_b$ and a fixed η with respect to G_0 on the horizontal axis and $\Omega \equiv 2\omega/\sqrt{\Gamma_a\Gamma_b}$ on the vertical axis. The solid lines are the imaginary parts of the poles.

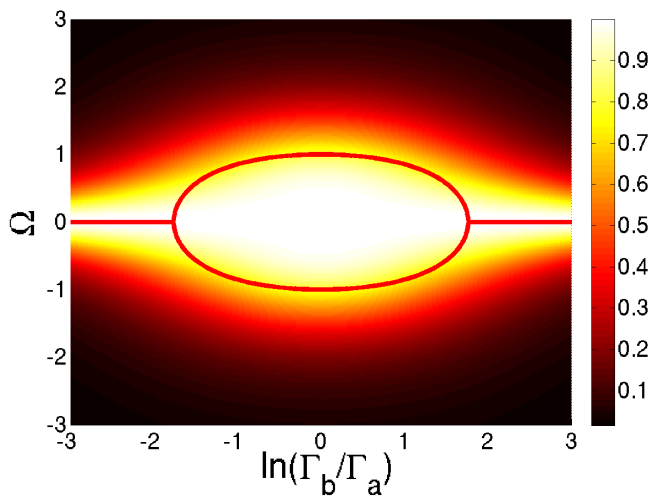


FIG. 6: (Color online). The color plot shows the conversion efficiency $R(\omega)/\eta$ at critical coupling ($G_0 = 1$) and a fixed η with respect to $\ln(\Gamma_b/\Gamma_a)$ on the horizontal axis and $\Omega \equiv 2\omega/\sqrt{\Gamma_a\Gamma_b}$ on the vertical axis. The solid lines are the imaginary parts of the poles. The bandwidth is maximum when $\Gamma_a = \Gamma_b$ and the imaginary parts of the poles are the farthest apart.

In the case of $\gamma'_{a,b} = 0$, $S_{AA'}$, $S_{AB'}$, $S_{BA'}$, and $S_{BB'}$ are all zero, and the ideal lossless beam-splitting relations are recovered:

$$\begin{pmatrix} \hat{A}_{\text{out}}(\omega) \\ \hat{B}_{\text{out}}(\omega) \end{pmatrix} = \begin{pmatrix} S_{AA}(-i\omega) & S_{AB}(-i\omega) \\ S_{BA}(-i\omega) & S_{BB}(-i\omega) \end{pmatrix} \begin{pmatrix} \hat{A}(\omega) \\ \hat{B}(\omega) \end{pmatrix}, \quad (3.25)$$

in which case the conversion efficiency at zero detuning can be perfect at critical coupling:

$$G_0 = 1, \quad R(0) = 1, \quad T(0) \equiv |S_{AA}(0)|^2 = |S_{BB}(0)|^2 = 0. \quad (3.26)$$

Faithful frequency conversion thus requires relatively low parasitic losses ($\gamma'_a \ll \gamma_a, \gamma'_b \ll \gamma_b$) and the critical coupling condition ($G_0 = 1$).

IV. BLUE-SIDEBAND OPTICAL PUMPING

A. Laplace analysis

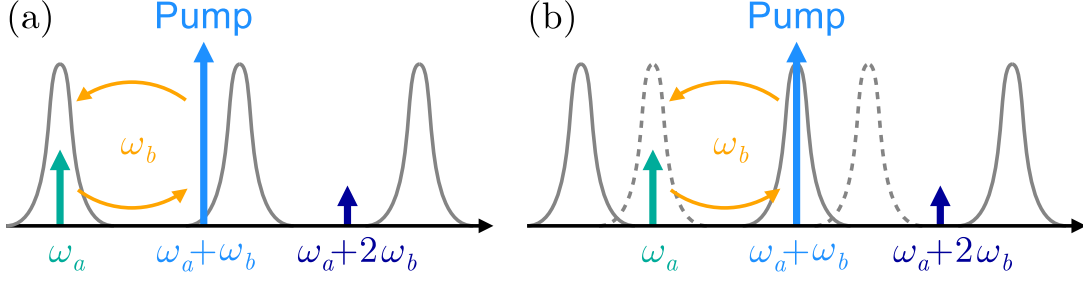


FIG. 7: (Color online). Blue-sideband optical pumping scheme in (a) a doubly-resonant configuration with an off-resonant pump and (b) a triply-resonant configuration with a resonant pump.

The analysis of a blue-sideband optical pumping scheme (Fig. 7) is similar; the equations of motion are now given by

$$\frac{da}{dt} = ig\alpha b^\dagger - \frac{\Gamma_a}{2}a + \sqrt{\gamma_a}A + \sqrt{\gamma'_a}A', \quad (4.1)$$

$$\frac{db}{dt} = ig\alpha a^\dagger - \frac{\Gamma_b}{2}b + \sqrt{\gamma_b}B + \sqrt{\gamma'_b}B', \quad (4.2)$$

$$A_{\text{out}} = \sqrt{\gamma_a}a - A, \quad (4.3)$$

$$B_{\text{out}} = \sqrt{\gamma_b}b - B. \quad (4.4)$$

The solutions for A_{out} and B_{out}^\dagger in the Laplace domain can be written as

$$\begin{pmatrix} \tilde{A}_{\text{out}}(s) \\ \tilde{B}_{\text{out}}^\dagger(s^*) \end{pmatrix} = \begin{pmatrix} \mathcal{F}_{Aa}(s) & \mathcal{F}_{Ab}(s) \\ \mathcal{F}_{Ba}(s) & \mathcal{F}_{Bb}(s) \end{pmatrix} \begin{pmatrix} a(0) \\ b^\dagger(0) \end{pmatrix} + \begin{pmatrix} \mathcal{S}_{AA}(s) & \mathcal{S}_{AB}(s) & \mathcal{S}_{AA'}(s) & \mathcal{S}_{AB'}(s) \\ \mathcal{S}_{BA}(s) & \mathcal{S}_{BB}(s) & \mathcal{S}_{BA'}(s) & \mathcal{S}_{BB'}(s) \end{pmatrix} \begin{pmatrix} \tilde{A}(s) \\ \tilde{B}^\dagger(s^*) \\ \tilde{A}'(s) \\ \tilde{B}'^\dagger(s^*) \end{pmatrix}. \quad (4.5)$$

These relations suggest that the electro-optic modulator now acts as a nondegenerate parametric amplifier. The \mathcal{F} matrix is

$$\mathcal{F}(s) = \frac{1}{\mathcal{D}(s)} \begin{pmatrix} \sqrt{\gamma_a}(s + \Gamma_b/2) & i\sqrt{\gamma_a}g\alpha \\ -i\sqrt{\gamma_a}g\alpha^* & \sqrt{\gamma_b}(s + \Gamma_a/2) \end{pmatrix}, \quad (4.6)$$

$$\mathcal{D}(s) \equiv \left(s + \frac{\Gamma_a}{2}\right) \left(s + \frac{\Gamma_b}{2}\right) - |g\alpha|^2 \quad (4.7)$$

$$= (s - \pi_+)(s - \pi_-). \quad (4.8)$$

The poles are

$$\pi_\pm = -\frac{\Gamma_a + \Gamma_b}{4} \pm \sqrt{\left(\frac{\Gamma_a - \Gamma_b}{4}\right)^2 + |g\alpha|^2}, \quad (4.9)$$

which, as shown in Fig. 8, follow very different loci than the ones for red-sideband pumping in Fig. 3 and remain real. When

$$G_0 \equiv \frac{4|g\alpha|^2}{\Gamma_a\Gamma_b} \geq 1, \quad \pi_+ \geq 0, \quad (4.10)$$

the π_+ pole moves to the right-half plane, and the system becomes unstable. In other words, $G_0 \geq 1$ is the threshold condition for electro-optic parametric *oscillation*.

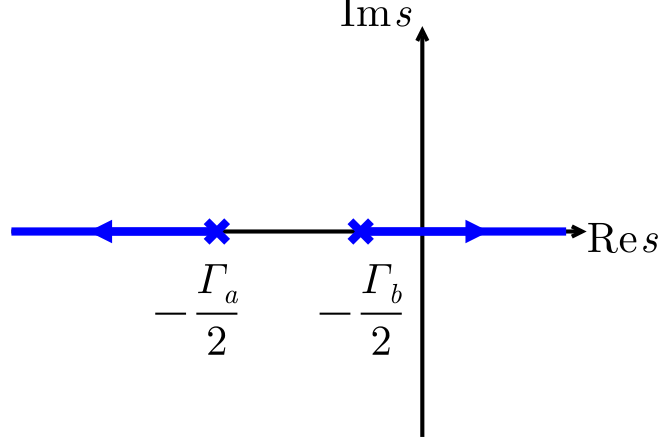


FIG. 8: (Color online). Root-locus plot for increasing blue-sideband pump strength $|g\alpha|$.

B. Electro-optic parametric amplification

Below threshold ($G_0 < 1$), the input-output relations for the nondegenerate parametric amplifier are

$$\mathcal{S}(s) = \frac{1}{\mathcal{D}(s)} \begin{pmatrix} \left(-s + \frac{\gamma_a - \gamma'_a}{2}\right) \left(s + \frac{\Gamma_b}{2}\right) + |g\alpha|^2 & ig\alpha\sqrt{\gamma_a\gamma_b} & \sqrt{\gamma_a\gamma'_a} \left(s + \frac{\Gamma_b}{2}\right) & ig\alpha\sqrt{\gamma_a\gamma'_b} \\ -ig\alpha^*\sqrt{\gamma_a\gamma_b} & \left(-s + \frac{\gamma_b - \gamma'_b}{2}\right) \left(s + \frac{\Gamma_a}{2}\right) + |g\alpha|^2 & -ig\alpha^*\sqrt{\gamma'_a\gamma_b} & \sqrt{\gamma_b\gamma'_b} \left(s + \frac{\Gamma_a}{2}\right) \end{pmatrix}. \quad (4.11)$$

The parametric gains in the spectral domain are given by

$$\begin{pmatrix} \hat{A}_{\text{out}}(\omega) \\ \hat{B}_{\text{out}}^\dagger(-\omega) \end{pmatrix} = \begin{pmatrix} \mathcal{S}_{AA}(-i\omega) & \mathcal{S}_{AB}(-i\omega) & \mathcal{S}_{AA'}(-i\omega) & \mathcal{S}_{AB'}(-i\omega) \\ \mathcal{S}_{BA}(-i\omega) & \mathcal{S}_{BB}(-i\omega) & \mathcal{S}_{BA'}(-i\omega) & \mathcal{S}_{BB'}(-i\omega) \end{pmatrix} \begin{pmatrix} \hat{A}(\omega) \\ \hat{B}^\dagger(-\omega) \\ \hat{A}'(\omega) \\ \hat{B}'^\dagger(-\omega) \end{pmatrix}. \quad (4.12)$$

In particular, the amplified electro-optic conversion efficiency, or the idler gain, is

$$\mathcal{R}(\omega) \equiv |\mathcal{S}_{BA}(-i\omega)|^2 = |\mathcal{S}_{AB}(-i\omega)|^2 \quad (4.13)$$

$$= \frac{|g\alpha|^2\gamma_a\gamma_b}{(\omega^2 + \pi_+^2)(\omega^2 + \pi_-^2)}. \quad (4.14)$$

With the real poles, the spectral behavior of the amplifier in general resembles a bandpass filter around zero detuning, at which the gain is

$$\mathcal{R}(0) = \frac{4\eta G_0}{(1 - G_0)^2}. \quad (4.15)$$

Figure 9 plots this function in dB against the cooperativity parameter G_0 . Unlike the conversion efficiency for red-sideband pumping in Fig. 4, the gain increases indefinitely for increasing G_0 until the threshold condition.

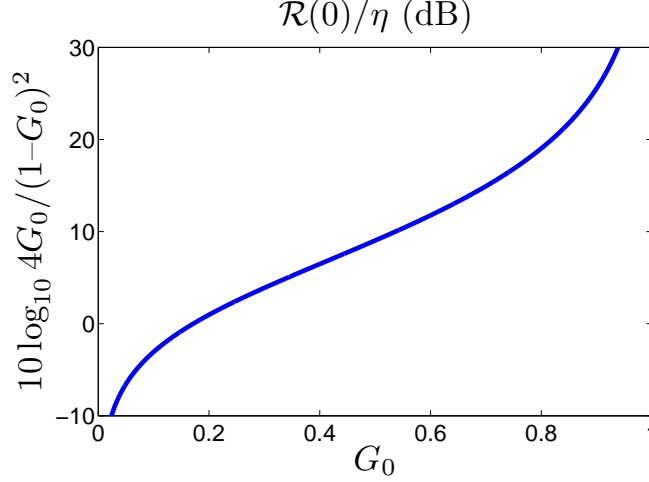


FIG. 9: (Color online). Idler gain $\mathcal{R}(0)/\eta$ in dB at zero detuning versus G_0 .

Parametric amplification may be useful for electro-optic conversion in the classical regime, but amplification in the quantum regime necessarily comes with noise. For coherent-state inputs, the noise statistics are completely determined by

$$\langle \hat{A}_{\text{out}}^\dagger(\omega) \hat{A}_{\text{out}}(\omega') \rangle = \langle \hat{A}_{\text{out}}^\dagger(\omega) \rangle \langle \hat{A}_{\text{out}}(\omega') \rangle + 2\pi\delta(\omega - \omega') [\mathcal{R}(\omega) + \mathcal{R}'_A(\omega)], \quad (4.16)$$

$$\langle \hat{B}_{\text{out}}^\dagger(\omega) \hat{B}_{\text{out}}(\omega') \rangle = \langle \hat{B}_{\text{out}}^\dagger(\omega) \rangle \langle \hat{B}_{\text{out}}(\omega') \rangle + 2\pi\delta(\omega - \omega') [\mathcal{R}(\omega) + \mathcal{R}'_B(\omega)], \quad (4.17)$$

$$\langle \hat{A}_{\text{out}}(\omega) \hat{B}_{\text{out}}(\omega') \rangle = \langle \hat{A}_{\text{out}}(\omega) \rangle \langle \hat{B}_{\text{out}}(\omega') \rangle + 2\pi\delta(\omega + \omega') \mathcal{K}(\omega), \quad (4.18)$$

where

$$\mathcal{R}'_A(\omega) \equiv |\mathcal{S}_{AB'}(-i\omega)|^2 = \frac{|g\alpha|^2 \gamma_a \gamma'_b}{(\omega^2 + \pi_+^2)(\omega^2 + \pi_-^2)}, \quad (4.19)$$

$$\mathcal{R}'_B(\omega) \equiv |\mathcal{S}_{BA'}(-i\omega)|^2 = \frac{|g\alpha|^2 \gamma'_a \gamma_b}{(\omega^2 + \pi_+^2)(\omega^2 + \pi_-^2)}, \quad (4.20)$$

$$\mathcal{K}(\omega) \equiv \mathcal{S}_{AA}(-i\omega) \mathcal{S}_{BA}^*(-i\omega) + \mathcal{S}_{AA'}(-i\omega) \mathcal{S}_{BA'}^*(-i\omega) \quad (4.21)$$

$$= \frac{ig\alpha\sqrt{\gamma_a\gamma_b}}{(\omega^2 + \pi_+^2)(\omega^2 + \pi_-^2)} \left[\left(i\omega + \frac{\Gamma_a}{2} \right) \left(-i\omega + \frac{\Gamma_b}{2} \right) + |g\alpha|^2 \right]. \quad (4.22)$$

To investigate the nonclassicality of the hybrid squeezed state when the inputs are vacuum, one can use the optical equivalence theorem [9] to write the phase-sensitive covariance as

$$\langle \hat{A}_{\text{out}}(\omega) \hat{B}_{\text{out}}(\omega') \rangle = \int D\mathcal{A} D\mathcal{B} P_{\text{out}}[\mathcal{A}, \mathcal{B}] \mathcal{A}(\omega) \mathcal{B}(\omega'), \quad (4.23)$$

where \mathcal{A} and \mathcal{B} are classical fields and $P_{\text{out}}[\mathcal{A}, \mathcal{B}]$ is the P functional for the output fields. If the P representation is nonnegative, the Cauchy-Schwarz inequality gives

$$\left| \langle \hat{A}_{\text{out}}(\omega) \hat{B}_{\text{out}}(\omega') \rangle \right|^2 \leq \int D\mathcal{A} D\mathcal{B} P_{\text{out}}[\mathcal{A}, \mathcal{B}] |\mathcal{A}(\omega)|^2 \int D\mathcal{A} D\mathcal{B} P_{\text{out}}[\mathcal{A}, \mathcal{B}] |\mathcal{B}(\omega')|^2 \quad (4.24)$$

$$= \langle \hat{A}_{\text{out}}^\dagger(\omega) \hat{A}_{\text{out}}(\omega) \rangle \langle \hat{B}_{\text{out}}^\dagger(\omega') \hat{B}_{\text{out}}(\omega') \rangle. \quad (4.25)$$

This implies that, for a classical state,

$$|\mathcal{K}(\omega)|^2 = \frac{1}{\eta} \mathcal{R}^2(\omega) + \mathcal{R}(\omega) \quad (4.26)$$

$$\leq [\mathcal{R}(\omega) + \mathcal{R}'_A(\omega)] [\mathcal{R}(\omega) + \mathcal{R}'_B(\omega)] \quad (4.27)$$

$$= \frac{1}{\eta} \mathcal{R}^2(\omega) \equiv |\mathcal{K}_c(\omega)|^2. \quad (4.28)$$

One can then define a nonclassicality parameter as

$$\Lambda(\omega) \equiv \ln \frac{|\mathcal{K}(\omega)|^2}{|\mathcal{K}_c(\omega)|^2} = \ln \left[1 + \frac{\eta}{\mathcal{R}(\omega)} \right]. \quad (4.29)$$

At zero detuning,

$$\Lambda(0) = \ln \frac{(1 + G_0)^2}{4G_0}, \quad (4.30)$$

which depends on G_0 but not η . The phase-sensitive correlation is strongly nonclassical ($\Lambda \gg 1$) when $G_0 \ll 1$ but vanishes at threshold, as shown in Fig. 10. The nonclassical correlation may be useful for quantum illumination [13, 14] in the microwave regime with a retained optical idler. Another electro-optic parametric amplifier may be used as a receiver that combines the return microwave signal and the optical idler and counts the optical photon number [15] to achieve quantum-enhanced target detection [13, 14] and secure communication [16].

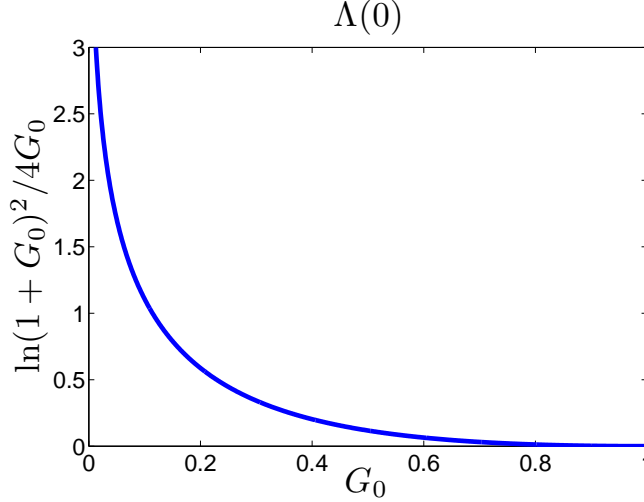


FIG. 10: (Color online). Nonclassicality parameter $\Lambda(0)$ at zero detuning versus G_0 .

In the case of $\gamma'_{a,b} = 0$, the ideal parametric-amplification relations are recovered:

$$\begin{pmatrix} \hat{A}_{\text{out}}(\omega) \\ \hat{B}_{\text{out}}^\dagger(-\omega) \end{pmatrix} = \begin{pmatrix} \mathcal{S}_{AA}(-i\omega) & \mathcal{S}_{AB}(-i\omega) \\ \mathcal{S}_{BA}(-i\omega) & \mathcal{S}_{BB}(-i\omega) \end{pmatrix} \begin{pmatrix} \hat{A}(\omega) \\ \hat{B}^\dagger(-\omega) \end{pmatrix}. \quad (4.31)$$

The standard analysis of two-mode parametric amplification and squeezing [17, 18] then applies.

C. Hybrid entangled photons

An alternative way of studying the entanglement between the two fields is to consider the Schrödinger picture. Assume that the idler gain is small enough such that one can write

$$\hat{A}_{\text{out}}(\omega) \approx \hat{A}(\omega) - i \left[\hat{A}(\omega), \epsilon \right], \quad (4.32)$$

ϵ being an Hermitian operator, and likewise for the other output fields. It is not difficult to show that this can be satisfied if $G_0 \ll 1$ and

$$\epsilon = \int_{-\infty}^{\infty} \frac{d\omega}{2\pi} \left[i\mathcal{S}_{AB}(-i\omega) \hat{A}^\dagger(\omega) \hat{B}^\dagger(-\omega) + i\mathcal{S}_{AB'}(-i\omega) \hat{A}^\dagger(\omega) \hat{B}'^\dagger(-\omega) + i\mathcal{S}_{B'A'}^*(-i\omega) \hat{A}'^\dagger(\omega) \hat{B}^\dagger(-\omega) + \text{H.c.} \right], \quad (4.33)$$

H.c. denoting the Hermitian conjugate. One can then write the unitary evolution operator as

$$U \approx 1 - i\epsilon, \quad (4.34)$$

and the Schrödinger-picture output state for a vacuum input state $|\text{vac}\rangle$ as

$$|\Psi\rangle = U|\text{vac}\rangle \approx (1 - i\epsilon)|\text{vac}\rangle \quad (4.35)$$

$$= |\text{vac}\rangle + \int_{-\infty}^{\infty} \frac{d\omega}{2\pi} \left[\mathcal{S}_{AB}(-i\omega)\hat{A}^\dagger(\omega)\hat{B}^\dagger(-\omega) + \mathcal{S}_{AB'}(-i\omega)\hat{A}^\dagger(\omega)\hat{B}'^\dagger(-\omega) + \mathcal{S}_{B'A'}^*(-i\omega)\hat{A}'^\dagger(\omega)\hat{B}^\dagger(-\omega) \right] |\text{vac}\rangle. \quad (4.36)$$

Tracing out the inaccessible A' and B' modes and denoting the vacuum state in the subspace of A and B modes as $|0, 0\rangle$, one obtains

$$\rho_{AB} = \text{tr}_{A'B'} |\Psi\rangle\langle\Psi| \quad (4.37)$$

$$\approx |\psi\rangle\langle\psi| + \int_{-\infty}^{\infty} \frac{d\omega}{2\pi} \mathcal{R}'_A(\omega) |1_\omega, 0\rangle\langle 1_\omega, 0| + \int_{-\infty}^{\infty} \frac{d\omega}{2\pi} \mathcal{R}'_B(\omega) |0, 1_\omega\rangle\langle 0, 1_\omega|, \quad (4.38)$$

$$|\psi\rangle \equiv |0, 0\rangle + \int_{-\infty}^{\infty} \frac{d\omega}{2\pi} \mathcal{S}_{AB}(-i\omega) |1_\omega, 1_{-\omega}\rangle, \quad (4.39)$$

where the unnormalized Fock states are defined by

$$|1_\omega, 0\rangle \equiv \hat{A}^\dagger(\omega)|0, 0\rangle, \quad (4.40)$$

$$|0, 1_\omega\rangle \equiv \hat{B}^\dagger(\omega)|0, 0\rangle, \quad (4.41)$$

$$|1_\omega, 1_{-\omega}\rangle \equiv \hat{A}^\dagger(\omega)\hat{B}^\dagger(-\omega)|0, 0\rangle. \quad (4.42)$$

Thus, $\mathcal{R}(\omega)$ is the entangled photon-pair generation rate per Hertz and $\mathcal{R}'_{A,B}(\omega)$ are the accidental photon generation rates per Hertz. If, for instance, an optical photon is used to herald a microwave photon, the heralding efficiency is

$$\frac{\mathcal{R}(\omega)}{\mathcal{R}'_A(\omega) + \mathcal{R}(\omega)} = \frac{\gamma_b}{\Gamma_b}, \quad (4.43)$$

which suggests that $\gamma'_a \ll \gamma_a$ and $\gamma'_b \ll \gamma_b$ are desirable for generating pure entangled photons. The entangled photons are frequency-anticorrelated, as one would expect from energy conservation.

V. CONCLUSION

The most important result of this paper is that efficient electro-optic frequency conversion requires the cooperativity parameter G_0 and the intrinsic efficiency η to be close to 1. While it should be possible to make η close to 1 using current microwave and optical resonator technology, the G_0 of existing devices [5] is unfortunately on the order of 10^{-5} only [8]. This should be enough for demonstrating hybrid entangled photons, if the electro-optic modulator is kept at a cryogenic temperature such that thermal microwave noise can be neglected, but the small G_0 is hardly useful for coherent frequency conversion. That said, given the potential room for improvement [8], which can make $g \sim 2\pi \times 5$ kHz and $G_0 \sim 5$ for achievable parameters, and the head start enjoyed by electro-optics technology [4, 5, 7] in experimental progress compared to competing electro-optomechanics proposals [2], which at this stage remain purely theoretical, one should remain cautiously optimistic about the future of quantum electro-optics.

Acknowledgments

Discussions with Jeffrey Shapiro, Carlton Caves, Aaron Danner, Olivier Pfister, Keith Schwab, Jun Ye, and James Thompson are gratefully acknowledged. This material is based on work supported in part by the Singapore National Research Foundation under NRF Award No. NRF-NRFF2011-07, NSF Grants No. PHY-0903953, and No. PHY-1005540.

[1] A. Wallraff *et al.*, Nature (London) **431**, 162 (2004); A. Blais *et al.*, Phys. Rev. A **69**, 062320 (2004); M. H. Devoret and J. M. Martinis, Quant. Inform. Process. **3**, 163 (2004), and references therein; J. Clarke and F. K. Wilhelm, Nature (London) **453**, 1031 (2008), and references therein.

- [2] L. Tian and H. Wang, *Phys. Rev. A* **82**, 053806 (2010); A. H. Safavi-Naeini and O. J. Painter, *New J. Phys.* **13**, 013017 (2011); C. A. Regal and K. W. Lehnert, *J. Phys.: Conf. Series* **264**, 012025 (2011).
- [3] A. Yariv, *Quantum Electronics* (Wiley, New York, 1989).
- [4] D. A. Cohen, M. Hossein-Zadeh, and A. F. J. Levi, *Electron. Lett.* **37**, 300 (2001); *Solid-State Electron.* **45**, 1577 (2001); D. A. Cohen and A. F. J. Levi, *Electron. Lett.* **37**, 37 (2001); *Solid State Electron.* **45**, 495 (2001).
- [5] V. S. Ilchenko *et al.*, *J. Opt. Soc. Am. B* **20**, 333 (2003).
- [6] A. B. Matsko *et al.*, *Opt. Express* **15**, 17401 (2007).
- [7] A. A. Savchenkov *et al.*, *Opt. Lett.* **34**, 1300 (2009); *IEEE Trans. Microw. Theor. Tech.* **58**, 3167 (2010).
- [8] M. Tsang, *Phys. Rev. A* **81**, 063837 (2010).
- [9] L. Mandel and E. Wolf, *Optical Coherence and Quantum Optics* (Cambridge University Press, Cambridge, 1995).
- [10] N. S. Nise, *Control Systems Engineering* (Wiley, New York, 2011).
- [11] S. M. Barnett *et al.*, *Phys. Rev. A* **57**, 2134 (1998).
- [12] H. J. Kimble, *Physica Scripta* **T76**, 127 (1998).
- [13] S. Lloyd, *Science* **321**, 1463 (2008).
- [14] S.-H. Tan *et al.*, *Phys. Rev. Lett.* **101**, 253601 (2008).
- [15] S. Guha and B. I. Erkmen, *Phys. Rev. A* **80**, 052310 (2009).
- [16] J. H. Shapiro, *Phys. Rev. A* **80**, 022320 (2009).
- [17] J. H. Shapiro and K. X. Sun, *J. Opt. Soc. Am. B* **11**, 1130 (1994); J. H. Shapiro, *Proc. SPIE* **5111**, 382 (2003).
- [18] C. M. Caves and B. L. Schumaker, *Phys. Rev. A* **31**, 3068 (1985); B. L. Schumaker and C. M. Caves, *ibid.* **31**, 3093 (1985).